

M. Mudelsee · K. Stattegger

## Exploring the structure of the mid-Pleistocene revolution with advanced methods of time-series analysis

Received: 8 July 1996 / Accepted: 18 December 1996

**Abstract** The mid-Pleistocene climate transition is a complex global change leading to Late Pleistocene ice ages with increased mean ice volume and dominant 100-ka cycle. A thorough understanding of this transition demands quantitative investigations in the time and frequency domains, and in the “stochastic domain”. Three methods of time-series analysis are presented which have been adapted for this purpose. They are tested by means of predefined, artificial time series and applied to benthic oxygen isotope ( $\delta^{18}\text{O}$ ) records which serve as ice volume indicator. Results are as follows: (a) The time-dependent mean shows an increase of 0.35‰ vs PDB from 942 to 892 ka. (b) Evolutionary spectral analysis reveals an abrupt increase of 100-ka cycle amplitude at approximately 650 ka. (c) Probability density function exhibits a bifurcation behavior at approximately 725 ka. These findings point to a multiple transition from a more linear climate system to a strong nonlinear system. The significant lead of the transition in mean, in relation to the 100-ka amplitude change and bifurcation is left open for explanation.

**Key words** Climate transition · Pleistocene · Oxygen isotopes · Time-dependent mean · Evolutionary spectral analysis · Probability density function

## Introduction

Oxygen isotope data from deep-sea sediment cores are widely used as a proxy for estimating ice volume and seawater temperatures in the geologic past. Astronomic

tuning of the isotope record, in addition to high-precision  $^{40}\text{Ar}/^{39}\text{Ar}$  ages, provides a time resolution down to a few thousand years on average for Plio-/Pleistocene sedimentary sequences. In such data, short-term changes are detectable in addition to long-term trends and oscillations.

In several deep-sea cores we observed the general cooling trend during the Pliocene corresponding to the formation of northern hemisphere’s ice cap which led to the “icehouse” state 2.5 million years ago (e.g., Shackleton et al. 1984; Raymo 1994; Tiedemann et al. 1994). The latest part of the Pliocene and the Quaternary period are characterized by large oscillations, abrupt changes, and further cooling in the Early Pleistocene. The mid-Pleistocene climate transition, sometimes called mid-Pleistocene revolution, which brought the system into the Late Pleistocene ice ages, consists of changes in both mean value (time domain) of ice volume, and in strength of the 100-ka cycle (frequency domain). Statements about timing of the mid-Pleistocene climate transition disagree, both concerning the position of the midpoint and the rate of change (Tables 1, 2).

To better define the transition, therefore, we undertook quantitative investigations in the time and frequency domains. In addition, we use the stochastic concept of time-dependent probability density function (PDF) which can exhibit bifurcation behavior. The PDF describes the distribution of the ice volume values (shape, range). Bifurcation means the transition from a one-modal density to a PDF with two distinct modes. Such a transition would indicate that the dynamic state of the climate system has changed. For example, unstable, irregular states may be attained by the system upon exceeding a threshold value for a certain climate parameter (e.g., Maasch and Saltzman 1990; Matteucci 1990; Saltzman 1990). Based on climate model analyses, the mid-Pleistocene climate transition has been considered as bifurcation behavior (Maasch and Saltzman 1990; Ghil 1994).

M. Mudelsee (✉) · K. Stattegger  
Geologisch-Paläontologisches Institut, Universität Kiel,  
Olshausenstrasse 40–60, D-24118 Kiel, Germany  
Fax: +49 431 880 4376  
e-mail: mam@zaphod.gpi.uni-kiel.de

**Table 1** Previous results (time domain) on the mid-Pleistocene climate transition, using  $\delta^{18}\text{O}$  records, compared with the results from this study

Mean	Standard deviation	Reference
Increase at 915 ka, duration: $\leq 50$ ka, amplitude: $< 0.36\text{‰}$	Increase at 915 ka	Prell (1982) <sup>a</sup>
Increase at 915 ka, duration: (abrupt), amplitude: $0.18\text{‰}$	Increase at 915 ka	Maasch (1988) <sup>a</sup>
Increase at 900 ka, duration: (abrupt)	Gradual increase (by a factor of $\sim 1.6$ ) between 1100 ka, or 850 ka, respectively, and 650 ka	DeBlonde and Peltier (1991)
Increase at 910 ka duration: 20 ka		Berger and Jansen (1994)
Increase at $917 \pm 19$ ka, duration: $50 \pm 10$ ka, amplitude: $0.35 \pm 0.07\text{‰}$	Increase (by a factor of $1.3 \pm 0.1$ ) at 850 ka, or 625 ka, respectively, duration: $275 \pm 35$ ka	This study <sup>b</sup>

<sup>a</sup> Quoted ages were corrected corresponding to an actualized magnetostratigraphic timescale (Top Jaramillo = 915 ka; Spell and McDougall 1992)

<sup>b</sup> Error quotations are  $1 \sigma$  of the weighted average (maximum of internal/external error). Since the errors of start and end time are positively correlated, the errors of duration and midpoint do not follow from simple error propagation, but are smaller. Based on the calculations in the "automatic mode" of the regression (see text), we used the following individual results for averaging. Mean: midpoint =  $920 \pm 35$  ka (DSDP 607) and  $915 \pm 23$  ka (ODP 659) respectively; duration =  $70 \pm 10$  ka (DSDP 607) and  $45 \pm 5$  ka (ODP 659), Standard deviation: midpoint =  $625 \pm 50$  ka (DSDP 607) and  $850 \pm 50$  ka (ODP 659), respectively; duration =  $250 \pm 50$  ka (DSDP 607) and  $300 \pm 50$  ka, respectively (ODP 659)

**Table 2** Previous results (frequency domain) on the mid-Pleistocene climate transition, using  $\delta^{18}\text{O}$  records, compared with the results from this study

100-ka amplitude	41-ka amplitude	Reference
Distinct increase at 900 ka	General increase from 1300 to 600 ka, marked decrease at 600 ka	Pisias and Moore (1981) <sup>a</sup>
Progressive increase from [940 ka; 1340 ka] to [0; 740 ka]		Pestiaux and Berger (1984) <sup>a</sup>
Clear increase from [550 ka; 1300 ka] to [0; 550 ka]	Nearly constant since 1300 ka	Shackleton et al. (1988) <sup>a</sup>
Increase between 920 and 750 ka, strong increase between 750 and 640 ka	Decrease between 1180 and 590 ka	Ruddiman et al. (1989) <sup>a</sup>
Gradual increase between 1250 and 620 ka	Gradual decrease between 1250 and 620 ka	Berger and Wefer (1992)
Increase at 1000 ka	Nearly constant since 3000 ka	Birchfield and Ghil (1993)
Gradual increase between 1000 and 500 ka	Decrease at 1000 ka	Park and Maasch (1993)
Increase between 1000 and 500 ka	Decrease between 1000 and 500 ka	Tiedemann et al. (1994)
Multi-step transition since 900 ka, strongest change at 750 ka	Persistent, through variable, since 2000 ka	Bolton et al. (1995) <sup>b</sup>
Abrupt increase at 700 ka	Abrupt decrease at 700 ka	Lau and Weng (1995) <sup>b</sup>
Abrupt increase at 650 ka	Nearly constant since 1100 ka	This study

<sup>a</sup> Quoted ages were corrected corresponding to an actual magnetostratigraphic timescale (Brunhes/Matuyama = 778 ka; Singer and Pringle 1996), Top Jaramillo = 915 ka (Spell and McDougall 1992), Base Jaramillo = 1010 ka (Spell and McDougall 1992), Cobb Mountain = 1172 ka (Spell and McDougall 1992; Turrin et al. 1994)

<sup>b</sup> Method: wavelet analysis

The Grassberger-Procaccia algorithm, another tool for analyzing nonlinear dynamic systems, was applied to oxygen isotope records in order to estimate the dimension of the Plio-/Pleistocene climate system (Mudelsee and Statteger 1994; Mudelsee 1995). The limited amount of data (less than ca. 1200 points) turned out to be a principal obstacle, allowing merely an estimated lower bound of approximately five significant climate variables.

In this paper, three methods of time-series analysis (time-dependent mean and standard deviation, evolutionary spectral analysis, time-dependent probability density function) are presented. By means of predefined, artificial time series the abilities of the methods and the uncertainties of the estimated parameters are evaluated. The structure of the mid-Pleistocene climate transition is explored by applying these methods to published benthic oxygen isotope records.

---

#### Data and methods

Oxygen isotope values, measured on benthic foraminifera, correspond mainly to continental ice volume (global signal) and to bottom-water temperatures (Emiliani 1955; Shackleton 1967). Mix (1987) discusses the global vs local signal proportion. The  $\delta^{18}\text{O}$  value is the permil-deviation of atomic ratio  $^{18}\text{O}/^{16}\text{O}$  of a sample with respect to a standard (PDB). Two high-resolution  $\delta^{18}\text{O}$  records from Deep Sea Drilling Project (DSDP) site 607 (Ruddiman et al. 1989; location  $41^\circ\text{N}$ ,  $33^\circ\text{W}$ , water depth 3427 m, the astronomically tuned timescale corresponds to that of Shackleton et al. 1990), and Ocean Drilling Program (ODP) site 659 (Tiedemann et al. 1994; location  $18^\circ\text{N}$ ,  $21^\circ\text{W}$ , water depth 3070 m, astronomically tuned timescale) provide basis for exploring the mid-Pleistocene climate transition.

The climate transition should be reflected by systematic changes in the following time-dependent statistical quantities: mean and standard deviation (std), amplitudes of predominant cycles (i.e., 41- and 100-ka cycle), and PDF. In order to detect bifurcation behavior, emphasis is laid on the number of modes of the PDF.

These climate records also contain the precession cycle ( $\sim 21$  ka) as well as other, unknown signal components, i.e., noise. Therefore, an averaging procedure is required to extract the principal signal and to reduce the noise. This averaging procedure is also necessary for estimating the time-dependent standard deviation. We choose a rectangular window which is shifted successively along the time axis. The data points within the window are used for estimating the statistical quantities. The accompanying time value is calculated as the average of the time values of the collected data points (Ezekiel 1950, p. 52; Tukey 1977, p. 307). The running rectangular window is a more objective procedure than

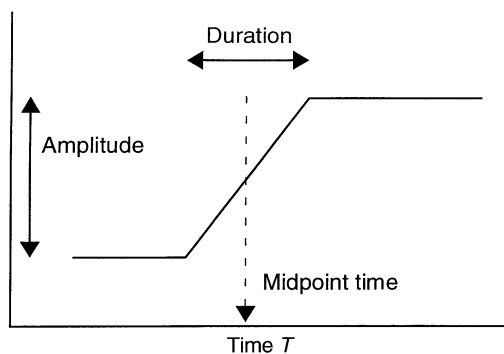


Fig. 1 Assumed ramp form of a transition; transition parameters

arbitrarily choosing certain distinct time intervals for comparison.

Since it is the most simple model to describe the rate of change, we assume a transition in the statistical quantities to be a “ramp function” (Fig. 1). Applied to measured time series, this assumption has to be examined for the presence of systematic errors. A drawback of a running average is the systematic broadening of a transition range due to the nonzero window width (see Fig. 2b). Hence, we face a trade-off problem (statistical vs systematic error). Our guidelines for the appropriate window width are explained separately for each method. It is important to test the methods by means of artificial time series, with predefined transitions in mean, standard deviation, 41- and 100-ka amplitude, or number of modes of PDF.

#### Time-dependent mean and standard deviation

The time-dependent mean quantifies the principal, longer-term climate course. The mid-Pleistocene climate transition is reflected by a transition in time-dependent mean towards higher ice volumes, i.e., higher  $\delta^{18}\text{O}$  values (Table 1). The temporal strength of the overlying climate fluctuations (Milankovitch and other deterministic fluctuations, and noise) is quantified by the time-dependent standard deviation.

The running rectangular window (width  $H$ ) smoothes overlying short-term fluctuations and reveals principal trends. This is illustrated by an artificial time series with an abrupt transition in mean (Fig. 2a). The reduction in the statistical error is, however, accompanied by a broadened ( $\pm H/2$ ) transition range (Fig. 2b), i.e., the duration appears longer than it is. In addition, the standard deviation shows enhanced values within  $\pm H/2$  around the transition range which do not correspond to enhanced fluctuations but result from the transition in mean (Fig. 2c).

In the case of the artificial time series (Fig. 2a), a value of  $H = 100$  ka has been found by means of Monte-Carlo simulations as best compromise between

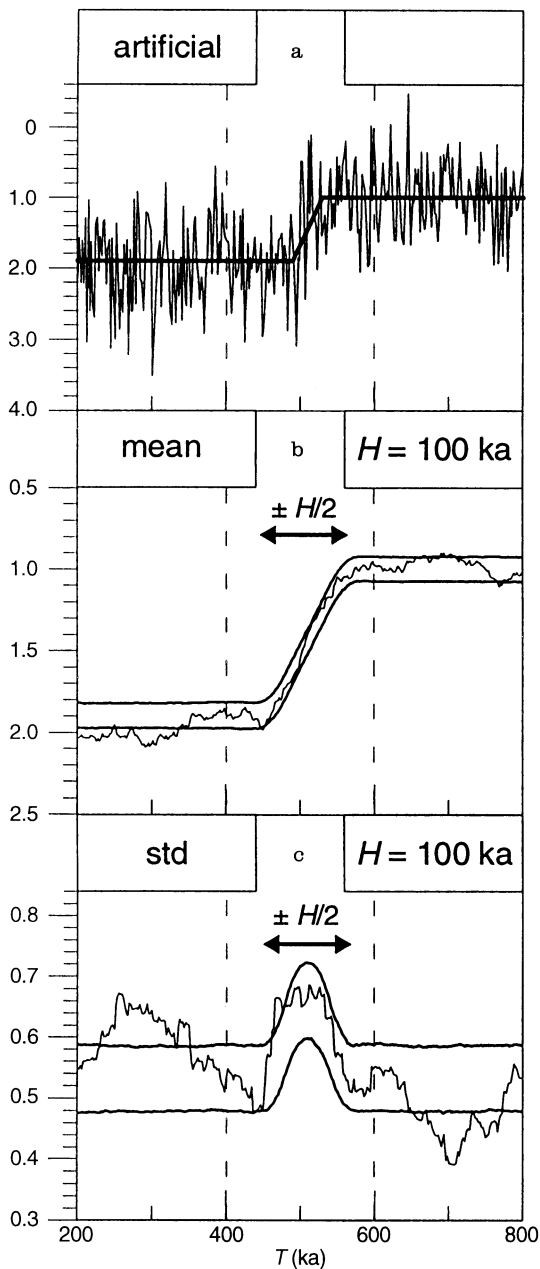


**Fig. 2a–c** Thin lines artificial time series with an abrupt, predefined transition in mean (from 1.0 to 2.0 at  $T = 500$  ka) and constant standard deviation (*std*; Gaussian noise of strength 0.5). The time resolution is 1 ka. **a** Unsmoothed presentation; **b, c** smoothed presentation of mean, and standard deviation, using a window of optimal width  $H = 100$  ka. Broadening of the transition range ( $\pm H/2$ ). Thick lines estimated transition (optimal solution) in unsmoothed presentation (**a**). In the smoothed presentation (**b, c**) the  $1 - \sigma$  error bands around the estimated optimal solution are shown. For estimated parameter values see text

statistical and systematic errors. In these simulations the optimal window width is determined by minimizing the absolute distance between a predefined transition and its estimate (Mudelsee 1995); hence, transitions should be best detectable. We carried out the simula-

tions for a variety of parameters (time resolution, duration of a transition, and signal/noise ratio, i.e., amplitude of a transition divided by the average standard deviation), since we expect the concept of optimal window width to be useful also for detecting and quantifying other climate transitions, e.g., the glaciation of the northern hemisphere (Mudelsee 1995).

In order to quantify the detected transition (midpoint time, duration, and amplitude) a three-phase regression (constant phase–linear phase–constant phase; see Fig. 1) is carried out on the original time-series points. In other words, different hypotheses about transitions in mean and standard deviation are examined. For this purpose, measures are used that compare a hypothetical course in mean, or standard deviation, with the original course in mean, or standard deviation. These measures constitute the sum of absolute deviations ( $L_1$  norm) between the respective courses. A minimized measure corresponds to optimal values for transition parameters. An error estimate for the parameter values is made by varying the values of transition parameters around their optimum and analyzing the influence on the measures. The regression is carried out twofold: In the first, interactive part the results from optimal smoothing (Fig. 2b, c) are recognized and the parameter values varied manually. This aids in detecting possible local minimum solutions of the measures. Secondly, in an automatic mode only midpoint time, and duration, respectively, of the hypothetical transition is varied, yielding more precise estimates and additional error estimates for these two crucial transition parameters. The methods used in previous studies (Table 1) estimate the duration only “by eye” and, further, provide no error estimation.

The result (optimal solution) for an artificial transition is presented in unsmoothed form (Fig. 2a). In the smoothed presentation (Fig. 2b, c) the  $1 - \sigma$  error bands around the optimal solution are shown which cover the true courses sufficiently. The optimal solution for the artificial transition (Fig. 2a) is estimated to consist in a transition from a mean of  $1.00 \pm 0.05$  at time  $T = 530 \pm 18$  ka to a mean of  $1.90 \pm 0.05$  at  $T = 490 \pm 18$  ka (all error quotations are  $1 \sigma$ ). The standard deviation is estimated to have a constant value of  $0.535 \pm 0.010$ . The result may be compared with the true parameter values (Fig. 2a).

The method is applied to the  $\delta^{18}\text{O}$  records from DSDP site 607 and ODP site 659. Since the temporal spacings of these time series (Figs. 3a and 4a) are larger than that of the artificial time series (Fig. 2a), and since the signal/noise ratio of the assumed transition is lower than that of the artificial time series, a higher value for optimal window width [ $H = 220$  ka (DSDP 607),  $H = 200$  ka (ODP 659)] results. In practice, we use a running mean over a number of points equal to  $H$  divided by the average temporal spacing. Since the time-series values are distributed nearly homogeneously on the time axis, the differences are negligible.

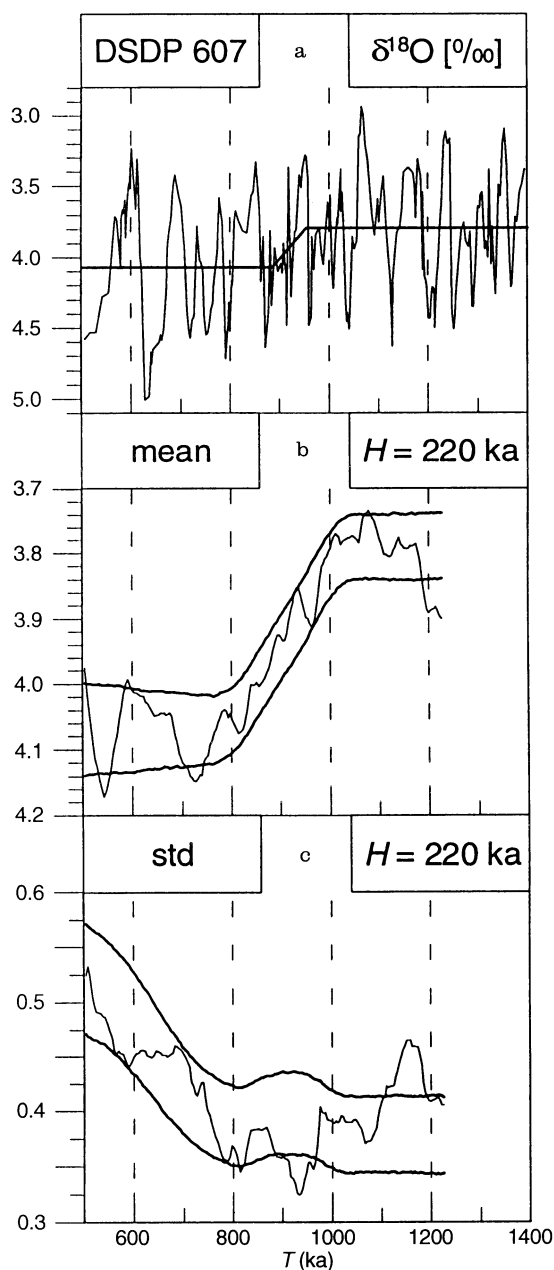


**Fig. 3a–c** Thin lines  $\delta^{18}\text{O}$  time series from DSDP site 607. The average time resolution within the plotted interval is 3.9 ka. **a** Unsmoothed presentation; **b**, **c** smoothed presentation of mean, and standard deviation (*std*), using a window of optimal width  $H = 220$  ka. Thick lines estimated transition (optimal solution) in unsmoothed presentation (**a**). In the smoothed presentation (**b**, **c**) the  $1 - \sigma$  error bands around the estimated optimal solution are shown. All units are ‰ vs PDB. For estimated parameter values see text

The result for the DSDP 607 time series (Fig. 3) shows no major systematic errors. In case of time-dependent mean, the  $1 - \sigma$  error band around the optimal solution, which consists of a transition from a mean  $\delta^{18}\text{O}$  of  $3.79 \pm 0.01\text{‰}$  at  $T = 955 \pm 35$  ka to a mean  $\delta^{18}\text{O}$  of  $4.07 \pm 0.01\text{‰}$  at  $T = 885 \pm 35$  ka, covers the true course (Fig. 3b). In the case of time-dependent

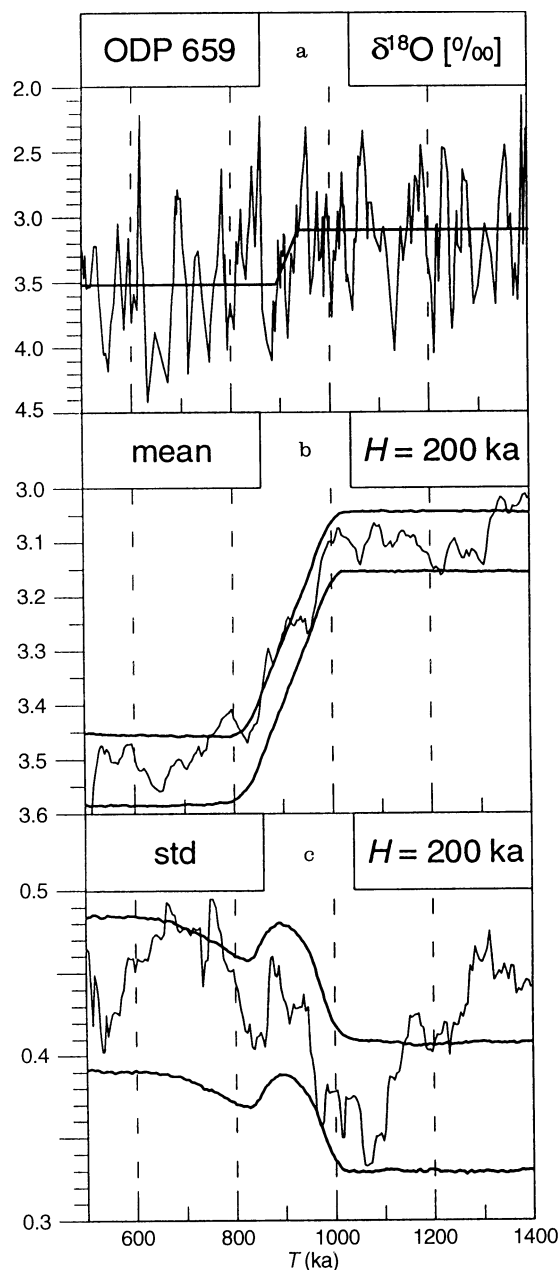


**Fig. 4a–c** Thin lines  $\delta^{18}\text{O}$  time series from ODP site 659. The average time resolution within the plotted interval is 4.7 ka. **a** Unsmoothed presentation; **b**, **c** smoothed presentation of mean, and standard deviation (*std*), using a window of optimal width  $H = 200$  ka. Thick lines estimated transition (optimal solution) in unsmoothed presentation (**a**). In the smoothed presentation (**b**, **c**) the  $1 - \sigma$  error bands around the estimated optimal solution are shown. All units are ‰ vs PDB. For estimated parameter values see text

standard deviation, an increase is estimated, from  $\text{std} = 0.38 \pm 0.01\text{‰}$  at  $T = 750 \pm 30$  ka to  $\text{std} = 0.55 \pm 0.05\text{‰}$  at  $T = 500 \pm 50$  ka (Fig. 3c). The systematic deviation in standard deviation for  $T > \text{ca. } 1100$  ka can be explained by the assumed ramp transition model (Fig. 1) which is too simple to model the course of standard deviation in the whole time interval.

The result for the ODP 659 time series (Fig. 4) also shows no major systematic errors. In the case of time-dependent mean, the  $1 - \sigma$  error band around the optimal solution, which consists of a transition from a mean  $\delta^{18}\text{O}$  of  $3.10 \pm 0.01\text{‰}$  at  $T = 937 \pm 23$  ka to a mean  $\delta^{18}\text{O}$  of  $3.52 \pm 0.01\text{‰}$  at  $T = 892 \pm 23$  ka, covers the true course (Fig. 4b). In the case of time-dependent standard deviation, a slow increase is estimated, from  $\text{std} = 0.37 \pm 0.01\text{‰}$  at  $T = 1000 \pm 50$  ka to  $\text{std} = 0.44 \pm 0.01\text{‰}$  at  $T = 700 \pm 50$  ka (Fig. 4c). The higher values around  $T = 900$  ka, due to the transition in mean, can successfully be modeled. The systematic deviation in standard deviation for  $T > \text{ca. } 1200$  ka can also be explained by the assumed ramp transition form. The average transition parameter values, calculated from the results for both time series, are summarized in Table 1.

### Evolutionary spectral analysis

The mid-Pleistocene climate transition also involves changes in the frequency domain (Table 2), namely from a mid-Pleistocene 41-ka cycle to a dominant 100-ka cycle in the Late Pleistocene. Therefore, the amplitude for each of these two cycles is studied in its temporal evolution.

For testing and validating purposes, an artificial time series is composed of 41- and 100-ka cycles with a transition from 41 ka dominance towards 100 ka dominance at  $T = 1000$  ka (Fig. 5a). A rectangular window is shifted along the time axis and the amplitudes of the two cycles estimated within. The estimation follows the algorithm of Ferraz-Mello (1981). Thereby the time series values,  $X(T)$ , are split into a part  $X_f(T)$  corresponding to frequency  $f$  and a remaining part  $X_r(T)$ . By least-squares sine/cosine fits the amplitudes of  $X_f(T)$ , for  $f = 1/(41 \text{ ka})$  and  $f = 1/(100 \text{ ka})$  are estimated. In contrast to the methods used in previous studies (Table 2), this method offers the advantage of directly processing the original, unevenly spaced data. No interpolation, which may distort spectral characteristics (e.g., Schulz 1996), is necessary. By visual inspection a window width of  $H = 400$  ka has been found as best compromise (statistical vs systematic error). The predefined amplitudes of 41- and 100-ka cycles (Fig. 5a) are estimated correctly (Fig. 5b, c). A broadening of the transition occurs due to the nonzero window width.

The application to the  $\delta^{18}\text{O}$  record from DSDP site 607 (Fig. 6a) shows an abrupt transition of 100-ka amplitude at  $T \approx 650$  ka (Fig. 6b), in accordance with Schulz (1996) who used the same data and a window of 500-ka width. The enhanced values at  $T \approx 1000$ – $1200$  ka are assessed as significant. The 41-ka amplitude is nearly constant since  $\sim 1100$  ka (Fig. 6c).

The application to the  $\delta^{18}\text{O}$  record from ODP site 659 (Fig. 7a) also shows an abrupt transition of 100-ka amplitude at  $T \approx 650$  ka (Fig. 7b). The enhanced values

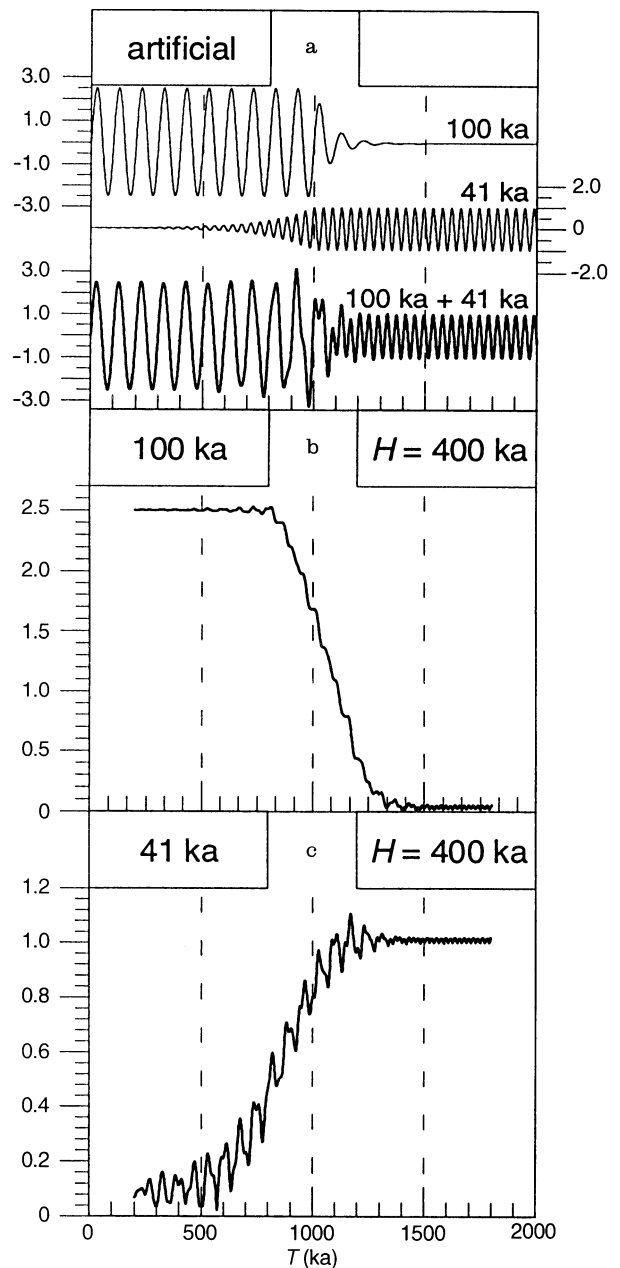


**Fig. 5** **a** Artificial time series (thick lines), composed of 100- and 41-ka signal components (thin lines), with a transition (41- to 100-ka dominance) at  $T = 1000$  ka. The time resolution is 1 ka. **b** Estimated temporal course of the amplitude of the 100-ka cycle, using a running window of width = 400 ka. **c** Same as **b** for the 41-ka cycle. Note broadening of estimated transition

at  $T \approx 1000$ – $1200$  ka are assessed as significant. The 41-ka amplitude likewise shows no pronounced transition (Fig. 7c). Possibly, lower values around  $T \approx 400$  and  $T \approx 1000$  ka are significant. In general, however, the mid-Pleistocene climate transition, in the frequency domain, consists of a pronounced, abrupt increase towards a dominant Late Pleistocene 100-ka cycle at  $T \approx 650$  ka. About the same results have been

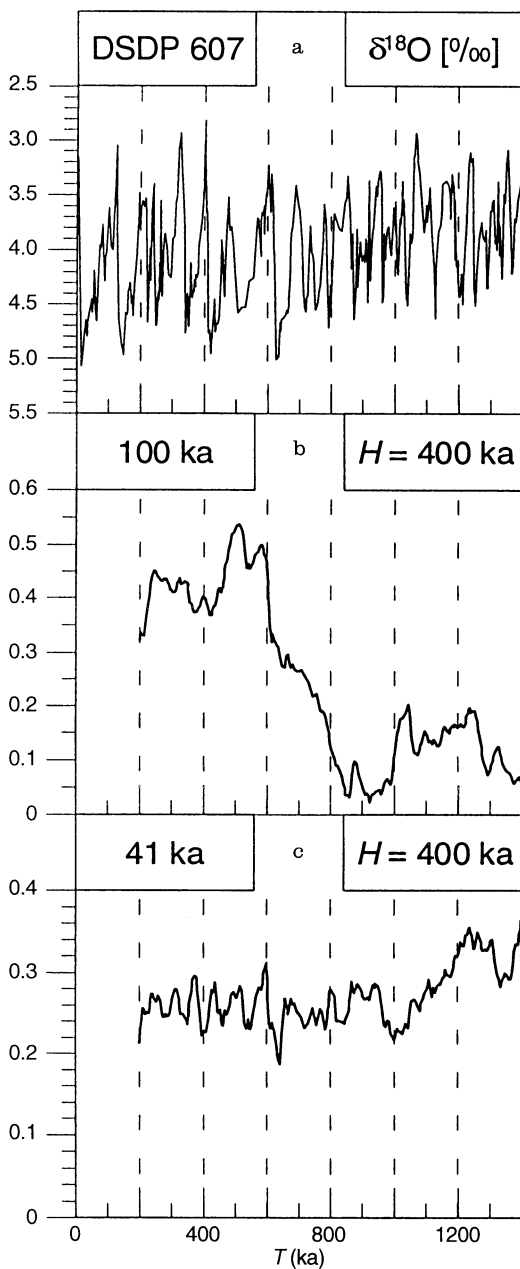


**Fig. 6** **a**  $\delta^{18}\text{O}$  time series from ODP site 607. The average time resolution within the plotted interval is 3.6 ka. **b** Estimated temporal course of the amplitude of the 100-ka cycle, using a running window of width = 400 ka. **c** Same as **b** for the 41-ka cycle. All units are ‰ vs PDB

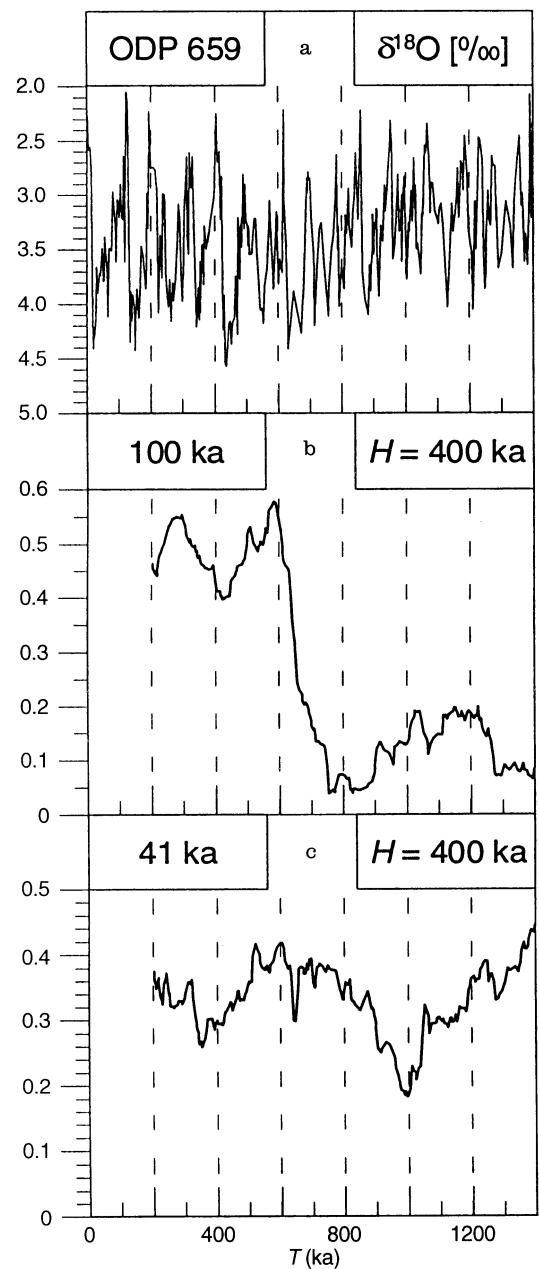


**Fig. 7** **a**  $\delta^{18}\text{O}$  time series from ODP site 659. The average time resolution within the plotted interval is 4.2 ka. **b** Estimated temporal course of the amplitude of the 100-ka cycle, using a running window of width = 400 ka. **c** Same as **b** for the 41-ka cycle. All units are ‰ vs PDB

obtained when using untuned timescales, with the exception of generally reduced 41-ka amplitudes (Mudelsee 1995).

#### Time-dependent probability density function

The probability density function,  $\text{PDF}(x)$ , denotes the chance to find a certain time-series value,  $X$ . Math-

ematically,  $\text{PDF}(x = X) \times \delta x$ , with  $\delta x \rightarrow 0$ , is the probability for a time-series value to lie within  $[X; X + \delta x]$ . In case of climate time series, the temporal evolution of the PDF (shape of the function, range of  $X$ -values) informs about the evolution of climate as a “statistical system” (e.g., Hasselmann 1976). Particularly, the number of modes of PDF is of interest since it can reveal bifurcation behavior (Maasch and Saltzman 1990; Matteucci 1990; Saltzman 1990; Ghil 1994), i.e., the

change from a one-modal PDF to a density function with two distinct modes.

The artificial time series (Fig. 8b) is derived in the lower part ([0; 500 ka]) from a predefined two-modal PDF (Fig. 8a), and in the upper part ([500 ka; 1000 ka]) from a three-modal PDF. A running window is used to investigate the temporal evolution of the PDF. A statistical test for the number of modes of PDF for the time series values within the window is performed. We enhanced further (Mudelsee 1995) the test of Silverman (1981, 1986) which is based on kernel density estimation and bootstrap simulation. [In addition to his test criterion for the number  $z$  of modes, namely (cf. Silverman 1986, p. 147), the proportion of samples generated from the estimated  $z$ -modal density  $PDF_z(x)$  which yield  $> z$  modes, we use the proportion of samples which yield  $\geq z$  modes when generated from  $PDF_z(x)$  and  $\leq z - 1$  modes when generated from  $PDF_{z-1}(x)$ . This should help to better estimate the true number of modes.] The number of points within the window must be held constant for yielding comparable results. We found a number of 200 points as good compromise between statistical demands and systematic errors (e.g., broadening of a transition). The statistical test allows

only to estimate the probability  $P$  that the number of modes is 2, 3, etc. The case of one mode is characterized by low values of  $P$ (two modes),  $P$ (three modes), etc. We made extensive test calculations with artificial time series to assess the power of the statistical test, i.e., the ability to detect certain predefined modes. We confirmed quantitatively that a higher number of modes, or a weaker separation between them, results in a reduced power (Mudelsee 1995). On the other hand, the test power increases with a larger number of data points.

The predefined change from three to two modes at  $T = 500$  ka (Fig. 8a, b) is detected by the statistical test to be at  $T \approx 550$  ka (Fig. 8d). This deviation is most likely due to the fact that the test is biased towards lower numbers of estimated modes. This test result allows an approximate error quantification ( $\sim 50$  ka) of the estimated transitions. The estimated PDFs (Fig. 8c) may be compared against the true PDFs (Fig. 8a).

Application of PDF analysis to the  $\delta^{18}\text{O}$  record DSDP 607, from which the time-dependent mean (compare above) has been subtracted, is shown in Fig. 9. This detrending is necessary in order to quantify the distribution of time series values around the

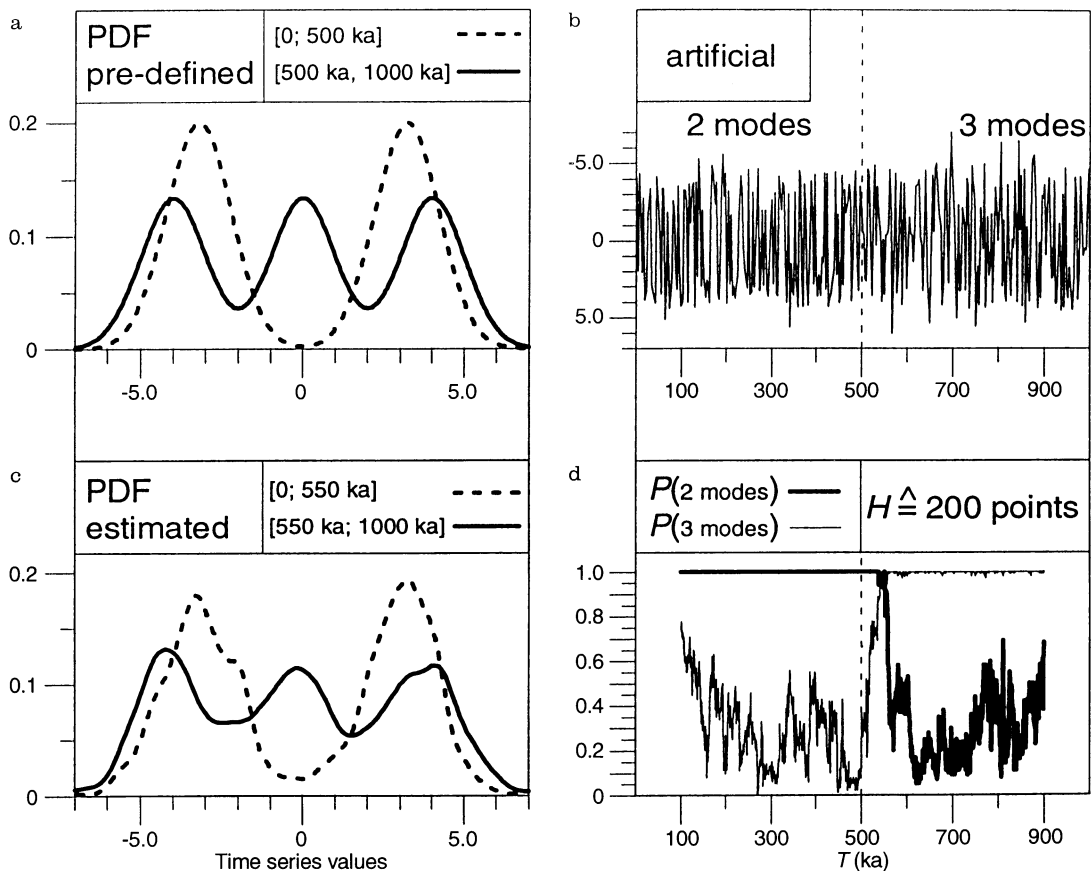


**Fig. 8** **b** Artificial time series, derived in [0; 500 ka] from the predefined two-modal probability density function (PDF) shown in **a**, in [500 ka; 1000 ka] from a three-modal PDF (**a**). The time resolution is 1 ka. Only every third point is plotted. **d** Estimated

probability for the number of modes of PDF against time. The test is carried out on a 200-point running window. **c** Estimated PDFs for the two detected time intervals



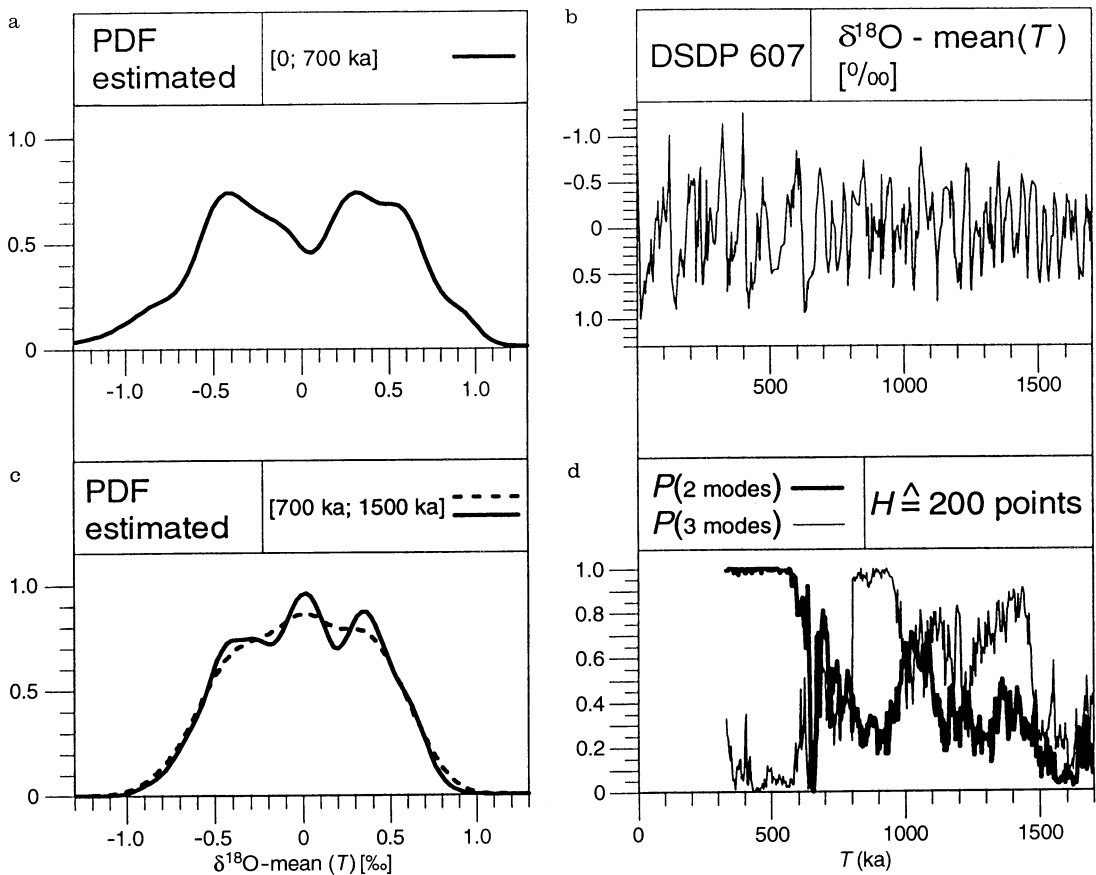


**Fig. 9** **b**  $\delta^{18}\text{O}$  time series from DSDP site 607 with subtracted time-dependent mean. The average time resolution within the plotted interval is 3.6 ka. **d** Estimated probability for the number of modes of PDF against time, using a 200-point running window. **a**, **c** Estimated PDFs [units: ( $\text{‰}$  vs PDB)/ka] for the two detected time intervals. For the interval [700 ka; 1500 ka] the one- and three-modal PDFs are plotted (**c**)

principal course, i.e., to prevent the broadening influence of a change in mean onto the PDF. The statistical test (Fig. 9d) clearly indicates a two-modal PDF for  $T < \text{ca. } 700 \text{ ka}$  (Fig. 9a). For  $T > \text{ca. } 700 \text{ ka}$  we have a broad, nearly one-modal density (Fig. 9c). Short intervals exist with a high  $P(\text{three modes})$  (Fig. 9d) and  $P(\text{four modes})$  (not shown). However, we are skeptical as to whether the number of data points allows detection of such a high number of modes. We could not divide the series into a higher number of shorter time intervals (each with a certain number of modes of PDF), because a lower number of data points would result in too low a power of the test. All estimated PDFs for the time interval [700 ka; 1500 ka] look similar (Fig. 9c, plotted for one and three modes). Therefore, we favor a broad PDF without small peaks (one modal) instead of a PDF with small, possibly spurious peaks (three or four modal).

The application to the  $\delta^{18}\text{O}$  record ODP 659, from which the time-dependent mean has been subtracted, is

shown in Fig. 10. The statistical test (Fig. 10d) indicates a three-modal PDF for  $T < \text{ca. } 750 \text{ ka}$  (Fig. 10a). For the interval [750 ka; 1350 ka] the test indicates a two-modal PDF (Fig. 10c). However, excluding the data point (860 ka,  $-1.3\text{‰}$ ; see Fig. 10b) and reanalyzing the time series yields a one-modal PDF for that time interval (not shown), without the mode at  $-1.31\text{‰}$  (see Fig. 10c). This means that this mode at  $-1.31\text{‰}$  is probably an artifact, due to a single point, caused by the “tendency for spurious noise to appear in the tails of the [kernel] estimates” (Silverman 1986, p. 18). Thus far, we have found one-modal mid-Pleistocene PDFs and multimodal PDFs for  $T < 700\text{--}750 \text{ ka}$ .

## Discussion

Our results on the mid-Pleistocene revolution in the time domain concur with the results from previous studies (Table 1) and, in addition, provide error estimates for the transition parameters. We find that on average the change in mean was at  $917 \pm 19 \text{ ka}$ , with a duration of  $50 \pm 10 \text{ ka}$ , and an amplitude (increased ice volume) of  $0.35 \pm 0.07\text{‰}$ . The change in standard deviation was more gradual. Higher values around 900 ka (Fig. 4c) should not be confused with a jump in

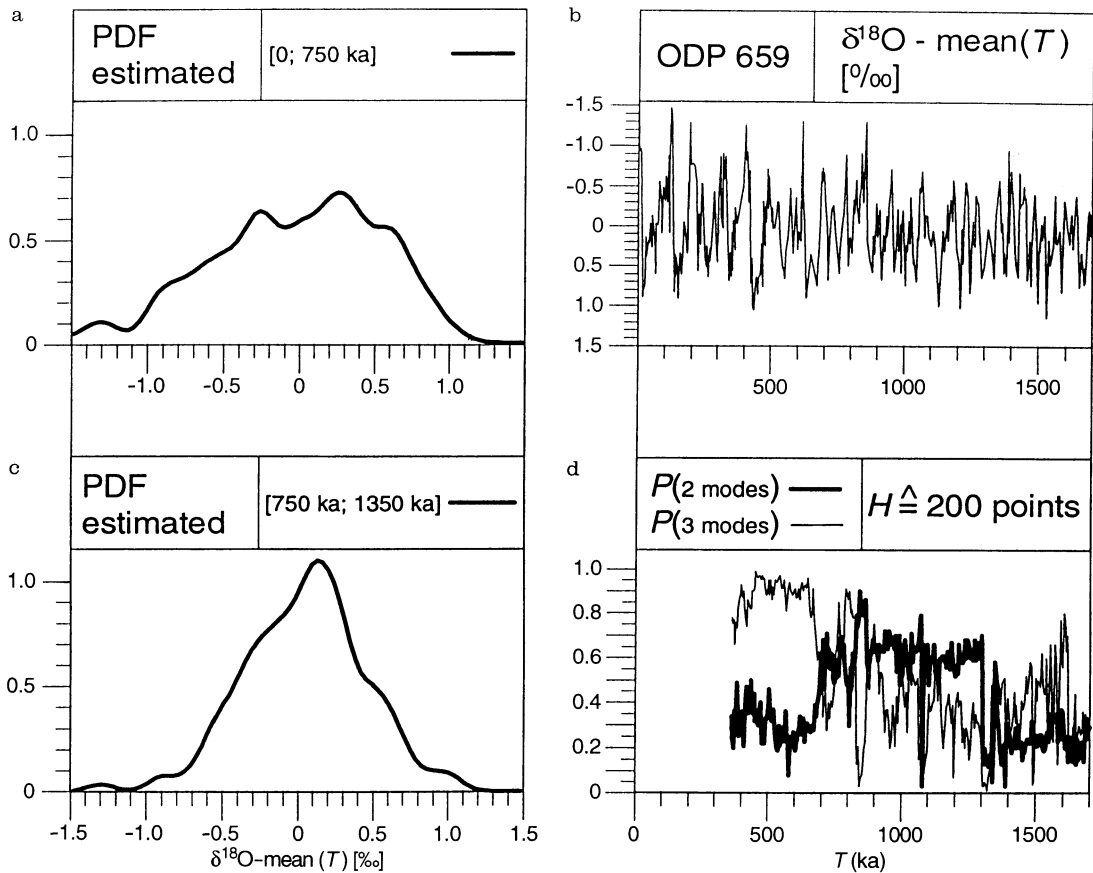


**Fig. 10** **b**  $\delta^{18}\text{O}$  time series from ODP site 659 with subtracted time-dependent mean. The average time resolution within the plotted interval is 4.2 ka. **d** Estimated probability for the number of modes of PDF against time, using a 200-point running window, **a**, **c** Estimated PDFs [units: (‰ vs PDB)/ka] for the two detected time intervals

standard deviation, since they are caused by the change in mean (see Fig. 2). Reliable estimates of the standard deviation transition midpoint require the investigation of more records. Our results in the frequency domain are in agreement with most of the results from previous studies (Table 2), particularly with those from studies using wavelet analysis. We consider this method and our method superior to choosing certain distinct time intervals for comparison, as was done in some studies listed in Table 2. In addition, other studies listed in Table 2 possibly have neglected the broadening influence when using a running window (see Fig. 5). Hence, an abrupt increase of 100-ka amplitude seems most likely to us, at  $T \approx 650$  ka. Time-dependent 41-ka amplitude appears not to have varied strongly since the Early Pleistocene. Possibly, an interval of stronger climate fluctuations was around  $T \approx 1200$  ka [higher 100-ka amplitude (Figs. 6b and 7b); higher 41-ka amplitude (Figs. 6c and 7c); higher standard deviation (Figs. 3c and 4c)]. We speculate that this interval was a first, but

unsuccessful, “attempt” of the climate system to attain a nonlinear “Late Pleistocene ice ages” state.

In the “stochastic domain” both records show a clear change in PDF at  $\sim 725$  ka. The DSDP 607 record exhibits bifurcation behavior which leads from a one-modal mid-Pleistocene PDF (Fig. 9c; we favor the one-modal PDF; see above) to a Late Pleistocene PDF with two distinct modes (at  $+0.31\text{‰}$  and  $-0.42\text{‰}$  relative to time-dependent mean; Fig. 9a).

Also the ODP 659 record shows a one-modal mid-Pleistocene PDF (Fig. 10c; the mode at  $-1.31\text{‰}$  is interpreted as artifact; see above). The Late Pleistocene PDF for this record has three modes (Fig. 10a), at  $+0.27$ ,  $-0.26$ , and  $-1.33\text{‰}$  relative to time-dependent mean. The latter of these modes corresponds to the interglacial extreme values of the time series (Fig. 10b). An additional analysis of the benthic  $\delta^{18}\text{O}$  record from the nearby located ODP site 658 (Sarnthein and Tiedemann 1990; location  $21^\circ\text{N}$ ,  $19^\circ\text{W}$ , water depth 2263 m, ages 0–728 ka, average temporal spacing 1.8 ka) revealed a three-modal Late Pleistocene PDF (not shown) similar to that of the ODP site 659 record, also with a mode corresponding to the interglacial extreme values. This feature of preferred interglacial values in the Late Pleistocene does not occur in the DSDP 607 record (Fig. 9a), and also not in the benthic  $\delta^{18}\text{O}$  record from ODP site 677 (Shackleton et al. 1990; location  $1^\circ\text{N}$ ,  $84^\circ\text{W}$ , water depth 3461 m) whose PDF

exhibits bifurcation behavior at approximately 800 ka (Mudelsee 1995). It is possibly a local feature of the subtropical deep East Atlantic, although we cannot offer a paleoceanographic explanation. As another possibility, it may be spurious noise in the tail of the PDF (compare above), introduced by the kernel density estimation method. Analyzing the PDFs with ordinary histogram method, using various bin widths, yielded no clear result on that possibility. A sampling bias, i.e., preferential sampling of interglacial sections of the ODP 658/659 sediment cores which could account for the “interglacial extreme” modes, seems unlikely since the linear correlation coefficient between depth spacing and  $\delta^{18}\text{O}$  value is zero for both cores. Independent of the cause of that feature, the global signal proportion of the  $\delta^{18}\text{O}$  record from ODP site 659 shows bifurcation behavior. However, separation of the Late Pleistocene PDF modes is weak (Fig. 10a).

The observed bimodality for Late Pleistocene global climate is considered to reflect a bistability generated by nonlinear climate processes (e.g., calving) which are able of transferring the system rapidly between a glacial and an interglacial mode (cf. Matteucci 1990). This bimodality is not caused by an eventual sinusoidal form of the signal since the corresponding modes are not located at the extreme values of the time series (Figs. 9b and 10b). In addition, the dominating Late Pleistocene  $\delta^{18}\text{O}$  signal, i.e., the 100-ka cycle, is sawtooth-shaped (Broecker and van Donk 1970; see Figs. 6a and 7a) than sinusoidal. Like any periodic function, the sawtooth has an uniform PDF. The bimodal structure, however, is blurred [broad PDF maxima (Fig. 9a); weak mode separation (Fig. 10a)] by fluctuations, which may indicate that a considerable number of climate variables are interacting.

The bifurcation behavior we observe at 700–750 ka is corroborated by Matteucci (1990) who found bifurcation in the SPECMAP standard  $\delta^{18}\text{O}$  record at 600 ka but, due to prechosen time intervals, regarded this timing as uncertain. A more accurate estimation of the bifurcation timing needs more records of still higher resolution to be investigated. Our result is further corroborated by Maasch and Saltzman (1990), Saltzman (1990), and Ghil (1994) who, based on climate model analyses, considered the mid-Pleistocene climate transition as a change from a principally linear to a complex, nonlinear climate system reflected by (rapid) changes in mean, standard deviation, periodicities, and bifurcation behavior.

Considering uncertainties in the timescales of climate records, estimation errors and powers of the statistical methods, as deduced from testing with artificial time series, we find that the transition in mean significantly leads the changes in 100-ka amplitude and PDF, by approximately 200–250 ka. These latter changes cannot be differentiated with sufficient temporal accuracy.

## Conclusions

The present study has revealed that the mid-Pleistocene climate transition is a multiple transition phenomenon. This has to be accounted for when considering physical explanations. In our view, the course of this global climate change towards Late Pleistocene ice ages is as follows (Fig. 11):

1. Pretransition,  $T \geq \text{ca. } 942 \text{ ka}$ . The 41-ka obliquity cycle accounts for a high proportion of signal variance. This cycle has a symmetric signal form (Ruddiman et al. 1986). The probability density is broad and approximately one-modal, and the climate fluctuations are centered around the mean value. All these observations point to a climate system which responds linearly to forcing.
2. Climate step,  $\text{ca. } 892 < T < \text{ca. } 942 \text{ ka}$ . This state is characterized by an increase in ice volume which lasted  $\sim 50 \text{ ka}$ . An explanation for this increase may be that atmospheric  $\text{CO}_2$  fell below a threshold value, permitting a higher rate of ice accumulation (Saltzman and Verbitsky 1993).

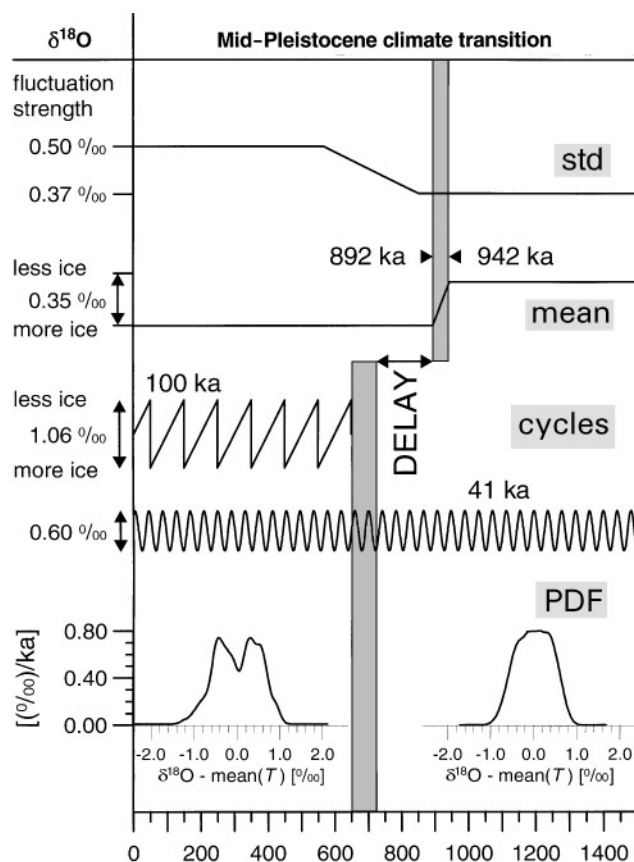


**Fig. 11** The mid-Pleistocene climate transition, as deduced from statistical analyses of  $\delta^{18}\text{O}$  time series, in schematic, simplified representation. A significant delay is ascertained between the change in mean, and the changes in amplitude of the 100-ka cycle and PDF. The amplitude of the 41-ka cycle may have overestimated due to the tuned timescales

3. Delay, ca. 650–725 ka  $\leq T \leq$  ca. 892 ka. The climate system “needs” this delay interval to “find” the two-modal solution after the initial disturbance in form of increased ice volume. Cyclicity (41 ka) still exists. We speculate that relaxation processes in some compartments of the climate system, e.g., bedrock (Emiliani and Geiss 1957), contribute to this delay. Currently, we are experimenting with an ice-bedrock climate model (Saltzman and Verbitsky 1993) to investigate the effects of a prescribed increase in ice accumulation rate (corresponding to the change in  $\delta^{18}\text{O}$  mean) on cyclicity evolution.
4. Late Pleistocene ice ages,  $T <$  ca. 650–725 ka. The 100-ka cycle starts nearly abruptly. This cycle has a sawtooth shape. The 41-ka cycle continues with no appreciable change in amplitude. The probability density function shows bifurcation behavior, leading to a Late Pleistocene density with two distinct modes. The climate fluctuations have become stronger (enhanced standard deviation). Two distinct dynamic solutions to external forcing and new boundary conditions are attained: strong glacials and interglacials. These findings indicate a climate system with a strong nonlinear character.

**Acknowledgements** We thank M. Schulz (SFB 313, Kiel, Germany) for discussions, providing his computer program for evolutionary spectral analysis, and reading a previous version of the manuscript. The constructive reviews by W.H. Berger (Scripps, La Jolla, Calif.) and L. Hinnov (Johns Hopkins University, Baltimore, Md.) on a previous version of this paper were helpful. M. Raymo (MIT, Cambridge, Mass.) and R. Tiedemann (GEOMAR, Kiel, Germany) kindly provided the oxygen-isotope records.

---

## References

- Berger WH, Wefer G (1992) Klimageschichte aus Tiefseesedimenten: Neues vom Ontong-Java-Plateau (Westpazifik). *Naturwissenschaften* 79: 541–550
- Berger WH, Jansen E (1994) Mid-Pleistocene climate shift: the Nansen connection. In: Johannessen OM, Muench RD, Overland JE (eds) *The polar oceans and their role in shaping the global environment*. *Geophys Monogr* 85: 295–311
- Birchfield GE, Ghil M (1993) Climate evolution in the Pliocene and Pleistocene from marine-sediment records and simulations: internal variability versus orbital forcing. *J Geophys Res* D98: 10385–10399
- Bolton EW, Maasch KA, Lilly JM (1995) A wavelet analysis of Plio-Pleistocene climate indicators: a new view of periodicity evolution. *Geophys Res Lett* 22: 2753–2756
- Broecker WS, van Donk J (1970) Insolation changes, ice volumes, and the  $\text{O}^{18}$  record in deep-sea cores. *Rev Geophys* 8: 169–198
- De Blonde G, Peltier WR (1991) A one-dimensional model of continental ice volume fluctuations through the Pleistocene: implications for the origin of the mid-Pleistocene climate transition. *J Climate* 4: 318–344
- Emiliani C (1955) Pleistocene temperatures. *J Geol* 63: 538–578
- Emiliani C, Geiss J (1957) On glaciations and their causes. *Geol Rundsch* 46: 576–601
- Ezekiel M (1950) *Methods of correlation analysis*, 2nd edn. Wiley, New York, pp 1–531
- Ferraz-Mello S (1981) Estimation of periods from unequally spaced observations. *Astronom J* 86: 619–624
- Ghil M (1994) Cryothermodynamics: the chaotic dynamics of paleoclimate. *Physica D* 77: 130–159
- Hasselmann K (1976) Stochastic climate models. Part I. Theory. *Tellus* 28: 473–485
- Lau K-M, Weng H (1995) Climate signal detection using wavelet transform: how to make a time series sing. *Bull Am Met Soc* 76: 2391–2402
- Maasch KA (1988) Statistical detection of the mid-Pleistocene transition. *Clim Dyn* 2: 133–143
- Maasch KA, Saltzman B (1990) A low-order dynamical model of global climatic variability over the full Pleistocene. *J. Geophys Res* D95: 1955–1963
- Matteucci G (1990) Analysis of the probability distribution of the late Pleistocene climatic record: implications for model validation. *Clim Dyn* 5: 35–52
- Mix AC (1987) The oxygen-isotope record of glaciation. In: Ruddiman WF, Wright HE Jr (eds) *North America and adjacent oceans during the last deglaciation*, vol K-3. *Geol Soc Am*, Boulder, Colorado, pp 111–135
- Mudelsee M (1995) *Entwicklung neuer statistischer Analysemethoden für Zeitreihen mariner, stabiler Isotopen: die Evolution des globalen Plio-/Pleistozänen Klimas*. Doctoral thesis, University of Kiel, pp 1–153
- Mudelsee M, Statterger K (1994) Plio-/Pleistocene climate modeling based on oxygen isotope time series from deep-sea sediment cores: The Grassberger-Procaccia algorithm and chaotic climatic systems. *Math Geol* 26: 799–815
- Park J, Maasch KA (1993) Plio-Pleistocene time evolution of the 100-kyr cycle in marine paleoclimatic records. *J Geophys Res* B98: 447–467
- Pestiaux P, Berger AL (1984) An optimal approach to the spectral characteristics of deep-sea climatic records. In: Berger A, Imbrie J, Hays J, Kukla G, Saltzman B (eds) *Milankovitch and climate*, part 1. Reidel, Dordrecht, pp 417–445
- Pisias NG, Moore TC Jr (1981) The evolution of Pleistocene climate: a time series approach. *Earth Planet* 52: 450–458
- Prell WL (1982) Oxygen and carbon isotope stratigraphy for the Quaternary of hole 502B: evidence for two modes of isotopic variability. In: Prell WL, Gardner JV et al. (eds) *Init Repts DSDP*, vol 68. U.S. Govt Printing Office, Washington DC, pp 455–464
- Raymo ME (1994) The initiation of northern hemisphere glaciation. *Annu Rev Earth Planet Sci* 22: 353–383
- Ruddiman WF, Raymo ME, McIntyre A (1986) Matuyama41 000-year cycles: North Atlantic Ocean and northern hemisphere ice sheets. *Earth Planet* 80: 117–129
- Ruddiman WF, Raymo ME, Martinson DG, Clement BM, Backman J (1989) Pleistocene evolution: northern hemisphere ice sheets and North Atlantic Ocean. *Paleoceanography* 4: 353–412
- Saltzman B (1990) Three basic problems of paleoclimatic modeling: a personal perspective and review. *Clim Dyn* 5: 67–78
- Saltzman B, Verbitsky MY (1993) Multiple instabilities and modes of glacial rhythmicity in the Plio-Pleistocene: a general theory of late Cenozoic climatic change. *Clim Dyn* 9: 1–15
- Sarnthein M, Tiedemann R (1990) Younger Dryas-style cooling events at glacial terminations I–VI at ODP site 658: associated benthic  $\delta^{13}\text{C}$  anomalies constrain meltwater hypothesis. *Paleoceanography* 5: 1041–1055
- Schulz M (1996) SPECTRUM und ENVELOPE: Computerprogramme zur Spektralanalyse nicht äquidistanter Zeitreihen. *Berichte Sonderforschungsbereich 313 (65)*: 1–131
- Shackleton NJ (1967) Oxygen isotope analyses and Pleistocene temperatures reassessed. *Nature* 215: 15–17
- Shackleton NJ, Backman J, Zimmerman H, Kent DV, Hall MA, Roberts DG, Schnitker D, Baldauf JG, Desprairies A,

- Homrighausen R, Huddleston P, Keene JB, Kaltenback AJ, Krumsiek KAO, Morton AC, Murray JW, Westberg-Smith J (1984) Oxygen isotope calibration of the onset of ice-rafting and history of glaciation in the North Atlantic region. *Nature* 307:620–623
- Shackleton NJ, Imbrie J, Pisias NG (1988) The evolution of oceanic oxygen-isotope variability in the North Atlantic over the past three million years. *Phil Trans R Soc Lond B* 318:679–686
- Shackleton NJ, Berger AL, Peltier WR (1990) An alternative astronomical calibration of the lower Pleistocene timescale based on ODP site 677. *Trans R Soc Edinb Earth Sci* 81:251–261
- Silverman BW (1981) Using kernel density estimates to investigate multimodality. *J R Sta B* 43:97–99
- Silverman BW (1986) Density estimation for statistics and data analysis. Chapman and Hall, London, pp 1–175
- Singer BS, Pringle MS (1996) Age and duration of the Matuyama-Brunhes geomagnetic polarity reversal from  $^{40}\text{Ar}/^{39}\text{Ar}$  incremental heating analyses of lavas. *Earth Planet* 139:47–61
- Spell TL, McDougall I (1992) Revisions to the age of the Brunhes-Matuyama boundary and the Pleistocene geomagnetic polarity timescale. *Geophys R L* 19:1181–1184
- Tiedemann R, Sarnthein M, Shackleton NJ (1994) Astronomic timescale for the Pliocene Atlantic  $\delta^{18}\text{O}$  and dust flux records of Ocean Drilling Program site 659. *Paleoceanography* 9:619–638
- Tukey JW (1977) *Exploratory data analysis*. Addison-Wesley, Reading, Massachusetts, pp 1–688
- Turrin BD, Donnelly-Nolan JM, Hearn BC Jr (1994)  $^{40}\text{Ar}/^{39}\text{Ar}$  ages from the rhyolite of Alder Creek, California: age of the Cobb Mountain normal-polarity subchron revisited. *Geology* 22:251–254